Chaos ARTICLE scitation.org/journal/cha

Patchy landscapes in arid environments: Nonlinear analysis of the interaction-redistribution model

Cite as: Chaos **30**, 093136 (2020); doi: 10.1063/5.0011010
Submitted: 26 May 2020 · Accepted: 24 August 2020 ·
Published Online: 21 September 2020

M. Messaoudi,[1,2] M. G. Clerc,[3] E. Berríos-Caro,[3] D. Pinto-Ramos,[3] M. Khaffou,[2] A. Makhoute,[1,2,a)] and M. Tlidi[1]

AFFILIATIONS

[1]Faculté des Sciences, Université Libre de Bruxelles (U.L.B), CP 231, Campus Plaine, B-1050 Bruxelles, Belgium
[2]Faculté des Sciences, Université Moulay Ismail, Dynamique des Systémes Complexes et Simulation Numérique, B.P. 11201, Zitoune, Meknès, Morocco
[3]Departamento de Física and Millennium Institute for Research in Optics, Facultad de Ciencias Físicas y Matemáticas, Universidad de Chile, Casilla 487-3, Santiago, Chile

Note: This article is part of the Focus Issue, instabilities and Nonequilibrium Structures.
[a)]**Author to whom correspondence should be addressed:** abdelkader.makhoute@ulb.ac.be

ABSTRACT

We consider a generic interaction-redistribution model of vegetation dynamics to investigate the formation of patchy vegetation in semi-arid and arid landscapes. First, we perform a weakly nonlinear analysis in the neighborhood of the symmetry-breaking instability. Following this analysis, we construct the bifurcation diagram of the biomass density. The weakly nonlinear analysis allows us to establish the condition under which the transition from super- to subcritical symmetry-breaking instability takes place. Second, we generate a random distribution of localized patches of vegetation numerically. This behavior occurs in regimes where a bare state coexists with a uniform biomass density. Field observations allow to estimate the total biomass density and the range of facilitative and competitive interactions.

How arid ecological systems experience transitions toward fragmentation of landscapes followed by desertification is an important ecological and biophysical question. Desertification is a major risk to the biological productivity of dryland zones. The lack of water induces hydric stress that prevents the formation of sustainable homogeneous vegetation cover and promotes a rather inhomogeneous distribution of vegetation. Since the biomass productivity of arid ecosystems is less compared to other ecosystems, they often attract little attention even though they cover more than 40% of the Earth's terrestrial area. Inhomogeneous distribution of vegetation of arid and semi-arid landscapes is the rule rather than the exception. It is now generally admitted that the spatial structuration of the biomass leading to the formation of vegetation patterns is attributed to facilitative and competitive interactions that affect the development of plants. More precisely, when the range of competitive interactions is longer than the facilitative ones, the homogeneous cover becomes unstable with respect to the symmetry-breaking instability leading to the formation of vegetation patterns constituted of spots of sparser vegetation. In this contribution in honor of Professor Enrique Tirapegui, we address the problem of vegetation pattern formation using a well-known interaction-redistribution model that focuses on the relationship between the structure of the individual plants and facilitation-competition interactions, as well as seed dispersion interactions existing within plant communities. Weakly nonlinear analysis of this model is presented. This analysis allows us to determine the threshold associated with the formation of localized spots or patches of vegetation. In order to perform parameter assessment, we provide results of field measurements of a peculiar case of vegetation, the alfa plant (or *Stipa tenacissima L.*).

I. INTRODUCTION

Vegetation of arid and semi-arid landscapes of the African, American, Asian, and Australian continents exhibits large spatial scale structures, generically called vegetation patterns.[1–3] They cover

about 40% of the Earth's terrestrial area. Either water-limited and/or nutrient-poor soils characterize these regions. In water-limited landscapes, the potential evaporation and transpiration of plants exceed the water supply provided by rainfalls. At small spatial scale, i.e., at the level of an individual plant, the water or nutrient scarcity induces a hydric stress that affects both the plant survival capacity and the plant growth. At large scale, i.e., at the community level, this stress provokes spatial landscape fragmentation. This adaptation to hydric stress involves a symmetry-breaking instability and self-organization, leading to the emergence of stable spatially periodic patterns.[4–6] The biomass has to self-organize in order to optimize the use of water or scarce resources. This is done through the well-known mechanism described by the interaction-redistribution model, consisting on a short range activation and long range inhibition. In general, the key features of vegetation pattern formation are the presence of two feedbacks. The first one corresponds to activation which is attributed to a positive feedback originated from the nonlocal facilitation that takes place at a shorter distance.[7] However, a short range activation alone cannot generate an increase of biomass production, and it is not sufficient to explain vegetation pattern formation. Then, a second feedback is necessary: the negative feedback that is caused by the competition between individuals plants for water and nutrients.[8] The theory based on the relationship between the structure of individual plants and the facilitation-competition interactions existing within plant communities[4–6] is in agreement with field observations.[9–11] Other approaches incorporate explicitly water transport by below-ground diffusion and/or above-ground run-off.[12–16] Further models are based on a discrete cellular automata.[17]

A well-documented example of vegetation pattern is the banded vegetation often called tiger bush. Thanks to the development of aerial photographs, this large-scale botanical organization was first observed in the early 1940s.[18] The spatial periodicity or wavelength is defined as the distance separating the middle of two successive bands of dense vegetation. Other types of vegetation pattern that have been observed include hexagonal or triangular periodic distributions of gaps ($H\pi$) or patches separated by bare soil (H0). When the aridity is increased, the following generic transition scenario can be predicted: $H\pi$-bands-H0.[5,19] Most of the modeling approaches mentioned above recover this transition sequence between vegetation patterns.

Vegetation patterns are not always periodic in space. The spatial distribution of vegetation cover may consist of isolated or randomly distributed patches or gaps. Such irregular patterns can involve groves within grasslands[20,21] or spots of bare soil within a grass matrix.[22] They consist of patches that are either isolated or in the form of clusters of patches. A typical example of patchy vegetation from Morocco is shown in Fig. 1(a). The vegetation is predominantly made up of the *Stipa tenacissima L.* plant, locally named "alfa." Vegetation localized pattern of Fig. 1(b) is obtained from numerical simulations of the interaction-redistribution model described by Eq. (3), which we will detail below. Another example of vegetation pattern involving large-scale gapped structures, often called fairy circles, belong to this class of localized vegetation patterns.[23] Several hypotheses have been proposed in the literature[22–33] to explain their formation. The mechanism leading to the formation of these mysterious fairy circles still remains an open problem. In both of the examples mentioned, such patterns have been interpreted as localized structures from the point of view of dynamical systems.[20,22] As in the case of periodic vegetation patterns, the aperiodic localized vegetation patterns are not specific to peculiar soils or plants. Localized vegetation patches or gaps may develop on soil ranging from sandy and salty to clayey, and the nature of vegetation may consist of grasses, shrubs, or trees.

Localized vegetation patches can be destabilized by the so-called curvature instability that affects the circular shape of the patches, followed by self-replication.[34–36] During the self-replication process, the biomass increases.[34,36] Recently, it has been shown that such a curvature instability may explain the formation of arcs and spirals of vegetation, even in isotropic environmental conditions.[37]

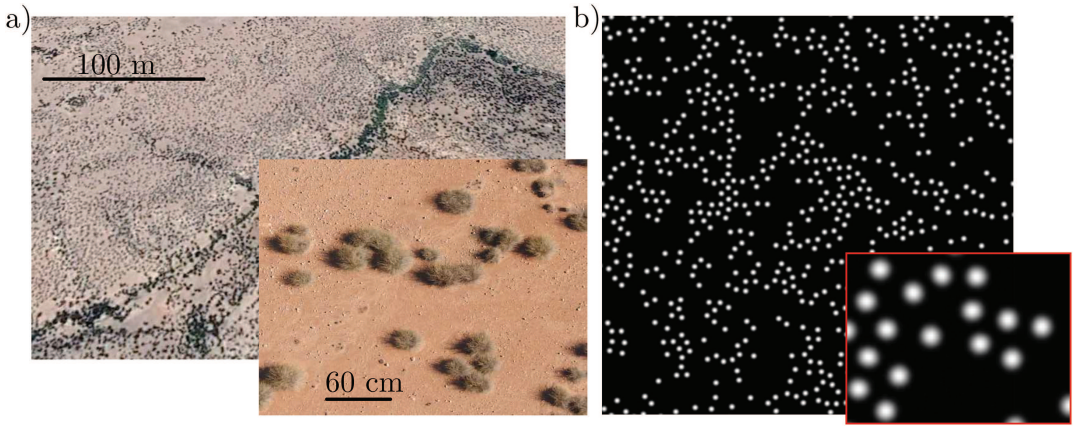

FIG. 1. Localized vegetation patterns. (a) Patchy landscape of Morocco (33° 6'22.79" N, 41° 21'33.43"O). (b) Vegetation pattern obtained by numerical simulations of Eq. (3). This consist of spots of dense vegetation (bright) surrounded by the bare state (dark). Parameters are $\kappa = -0.1$, $\gamma = 2$, $\delta = 0.2$, and $\alpha = 0.5$.

All the aforementioned cases show that the formation of localized patterns and pattern formation is an important issue not only in the context of plant ecology and environmental science but is also a multidisciplinary area of research in nonlinear science, involving physics, chemistry, and mathematics.[38–49]

In the first part of this work, we focus on the monostable regime, a regime far from a tipping point. In this regime, a single homogeneous cover can be destabilized via a symmetry-breaking instability leading to an emergence of vegetation patterns. A portion of the homogeneous cover undergoes two symmetry breaking instabilities characterized by different wavelengths. A wavelength of a given vegetation pattern is defined as the average distance between two successive maxima of the biomass. We perform a weakly nonlinear analysis in the vicinity of the above mentioned symmetry-breaking instabilities. This analysis allows us to determine a condition under which the modulational instability appears subcritically. In the second part of this work, we present recent field measurements of the alfa plant, or *Stipa tenacissima L.*, in the the center-south of Morocco. This plant is native to the northwestern Africa and the southern part of the Iberian Peninsula. Measurements of both fresh and dry above-ground biomass are provided, as well as the range of facilitation interaction between plants. By digging and extracting the whole biomass above the ground, we provide an estimation of the above-ground biomass and the length of competitive interaction.

This contribution is organized as follows. After a brief review of both periodic and localized vegetation patterns in arid and semi-arid landscapes, we present in Sec. II, a simple interaction-reduction model that has been widely used in the literature. In Sec. III, a weakly nonlinear analysis in the neighborhood of the symmetry-breaking instability is provided and the bifurcation diagram of the biomass density is constructed. In Sec. IV, we focus on a subcritical symmetry-breaking instability regime and we analyze the formation of localized aperiodic vegetation patches. In Sec. V, we conclude and discuss possible experimental verifications by field measurements of the alpha vegetation of high steppe plateau in eastern Morocco.

II. INTERACTION-REDISTRIBUTION MODEL

We consider a single state variable describing the time-space evolution of the biomass. This variable is described by the so-called interaction-redistribution model, which is based on the relationship between the structure of the individual plants and the facilitation-competition interactions, and seed dispersion interactions operating within plant communities. This modeling approach does not assume a peculiar plant or soil. Vegetation may consist of grasses, shrubs, or trees. Moreover, vegetation patterns may also develop on landscapes ranging from sandy and silty to clayey. This general framework of modeling supposes additionally that the environment is homogeneous and isotropic. The space-time evolution of the vegetation is described in terms of biomass. The total biomass involves two parts: the above- and the below-ground biomasses.

The spatiotemporal evolution of the normalized total biomass $b(\mathbf{r}, \mathbf{t})$ obeys the following integrodifferential equation:[22]

$$\partial_t b = b\left(1-b\right)\mathscr{M}_f - \mu b\mathscr{M}_c + D\mathscr{M}_d. \tag{1}$$

Time has been scaled such that the characteristic time of the growth process is unity. The first term in the right-hand side models the rate at which the biomass increases due to dissemination, germination, and other natural factors that tend to increase the biomass. The logistic term $(1-b)$ describes the fact that the biomass cannot exceed the carrying capacity. The second term models the biomass losses due to death or destruction by grazing, fire, termites, or herbivores. The third term models seed dispersion where D is the rate at which plants diffuse. The plant-to-plant facilitative $\mathscr{M}_f(\mathbf{r}, t)$, competitive $\mathscr{M}_c(\mathbf{r}, t)$ and seed dispersion $\mathscr{M}_d(\mathbf{r}, t)$ nonlocal interactions are

$$\mathscr{M}_{f,c}(\mathbf{r}, t) = \exp\left(\chi_{f,c}\int \phi_{f,c} b(|\mathbf{r}+\mathbf{r'}|, t, L_{f,c})\, d\mathbf{r'}\right),$$
$$\mathscr{M}_d = \int \left[\phi_{in} b(|\mathbf{r}+\mathbf{r'}|, t, L_d) - \phi_{out} b(|\mathbf{r'}|, t, L_d)\right] d\mathbf{r'}. \tag{2}$$

The nonlocal function $\mathscr{M}_f(\mathbf{r}, t)$ describes interactions facilitating the growth of the biomass density. This positive feedback operates over a distance L_f of the order of the plant's aerial structures (the radius of the crown or the canopy) involving, in particular, a reciprocal sheltering of neighboring plants against arid climatic conditions. The nonlocal function $\mathscr{M}_c(\mathbf{r}, t)$ models the plant-to-plant competitive interactions that on the contrary tends to enhance biomass decay. This negative feedback operates over distances of the order of the size of roots, i.e., the rhizosphere radius L_c. The parameters $\chi_{f,c}$ are the interaction strength associated with facilitation and competition, respectively. Both Kernels are normalized such that $\int \phi_{f,c}\, \mathrm{d}\mathbf{r'} = 1$, where the integral extends to the whole territory in two dimensions (assumed unbounded). The coefficient μ is the aridity parameter. The functions Φ_{in} and Φ_{out} are the dispersion kernels weighting the incoming and outgoing seed fluxes between neighboring plants according to their distance $|\mathbf{r}'|$. The seed dispersion kernels operate over a range L_d.

In what follows, we explore the dynamics in the neighborhood of the critical point associated with bistability also called the Lifshitz point of Eq. (1) satisfying the two conditions $\mathrm{d}\mu/\mathrm{d}b = 0$ and $\mathrm{d}^2\mu/\mathrm{d}^2 b = 0$. The coordinates of this point are $b = 0$, $\mu = 1$, and $\chi_f = 1 + \chi_c$. By using a multiple time scale expansions in the neighborhood of this critical point as $\mu = 1 + \kappa\zeta/2 + \cdots$, $b(\mathbf{r}, t) = \zeta^{1/2} u(\mathbf{r}, t) + \cdots$, and $\chi_c = \chi_0 + \chi\zeta^{1/4}$, where ζ is a small parameter that measures the distance from criticality. In addition, we assume that the diffusion coefficient is small, i.e., $D = p\zeta^{3/4}$. The application of the solvability condition at higher order inhomogeneous problem leads to the following partial differential equation:[5,22]

$$\partial_t u = -u(\eta - \kappa u + u^2) + (\delta - \gamma u)\nabla^2 u - \alpha u \nabla^4 u. \tag{3}$$

This equation is valid when the average biomass is low and the wavelength of the pattern is large (so that the pattern wavelength is much longer than the size of the plants). In this double limit, three parameters control the space-time evolution of the biomass: the aridity parameter η, which measures that account for the decrease-to-growth, κ, which is the facilitation-to-competition susceptibility rate ratio, and δ, which is the diffusion coefficient which assumed to be small. The parameters γ and α correspond to the nonlinear diffusion coefficients. The operators ∇^2 and the ∇^4 are the two-dimensional Laplacian and bi-Laplacian acting on a flat topography

whose spatial coordinates are (x, y). It has been shown recently that Eq. (3) holds for any shape of Kernels provided that their Taylor series converge.[61]

To determine the parameters δ, γ, and α appearing in Eq. (3), we need to specify the form of the Kernels describing the nonlocal interactions. In the case of Gaussian Kernel, we set $\phi_f = \exp(-|\mathbf{r'}|^2)/\pi$, $\phi_c = \epsilon_1 \exp(-\epsilon_1|\mathbf{r'}|^2)/\pi$, and $\phi_{in} = \epsilon_2 \exp(-\epsilon_2|\mathbf{r'}|^2)/\pi$ with $\epsilon_1 = L_f^2/L_c^2$ and $\epsilon_2 = L_f^2/L_d^2$, where L_d is the length associated with seed dispersion. Using the multiple time scale analysis explained above, we identify the following coefficients from Eq. (3):

$$\delta = \frac{p}{2\epsilon_2}, \ \gamma = \frac{\chi(1-\epsilon_1)}{2\epsilon_1}, \text{ and } \alpha = \frac{1}{16\epsilon_1}. \tag{4}$$

Equation (3) is derived in a low density and weak gradient limit from a generalized logistic equation with nonlocal facilitative, competitive, and seed dispersion interactions.[22] The most salient feature of Eq. (3) is the fact that the vegetation effective diffusion coefficient, i.e., $(\delta - \gamma u)$, which multiplies the Laplace operator term may become negative. This sign change in the effective diffusion tends to destabilize the spatial uniformity of the vegetation biomass. In contrast, the factor multiplying the double Laplacian, the bi-Laplacian term in the above equation, is always stabilizing. This terms insures the bounded growth of local (small) heterogeneities. Hence, the effective coefficient of the Laplacian term, i.e., $(\delta - \gamma u)$, dictates the stability of the system. When this term is negative, the system tends to destabilize the spatial uniformity of the vegetation biomass and vice versa. Equation (3) resembles a variational Swift–Hohenberg that is regularly derived in spatially extended systems. However, the presence of nonlinear diffusion terms $u\nabla^2 u$ and $u\nabla^4 u$ renders Eq. (3) non-gradient or non-variational.

The homogeneous and stationary equilibriums solution of Eq. (3) are $u_0 = 0$ and u_s, which fulfills

$$\eta = \kappa u_s - u_s^2, \tag{5}$$

the solution of this simple equation is $u_\pm = (\kappa \pm \sqrt{\kappa^2 - 4\eta})/2$. The solution $u_0 = 0$ models the state totally devoid of vegetation, i.e., bare state. The state u_+ corresponds to the uniform biomass density. When the parameter κ is positive, there exists a tipping point or a saddle-node bifurcation at $\eta_c = \kappa^2/4$, and the corresponding biomass is $u_c = \kappa/2$. The homogeneous cover u_- connecting the bare state and the upper homogeneous cover is always unstable. In what follows, we focus on the monostable regime, i.e., $\kappa < 0$. In this case, the state u_- is not physical since the biomass is a positive definite quantity, thus the only physically acceptable uniform solutions are the bare $u_0 = 0$ and the uniform cover u_+. Its linear stability analysis with respect to small perturbations (which do not break the ecosystem spatial uniformity) indicates that the bare state is unstable only when $\eta < 0$ and stable when $\eta > 0$. When the aridity parameter is increased, the uniform biomass decreases monotonously until reaches the bare state at $\eta = 0$. This state is stable when $\eta < 0$ and do not exist for $\eta < 0$.

The symmetry-breaking instability at which the homogeneous steady solution becomes unstable with respect to spatial fluctuations.

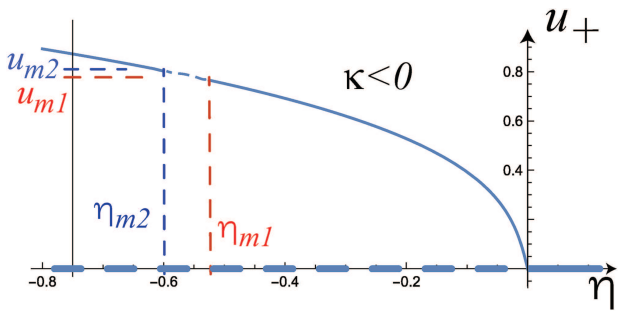

FIG. 2. Homogeneous steady state u_+ as a function of the aridity parameter η in the monostable case $\kappa < 0$. A portion of unstable cover is represented by a broken line. Parameters are $\kappa = -0.1$, $\gamma = 2$, $\delta = 0.2$, and $\alpha = 0.5$. For these parameters, the thresholds are $\eta_{m1} = -0.52$, $u_{m1} = 0.68$, $\eta_{m2} = -0.05$, and $u_{m2} = 0.20$.

At these bifurcation points the wavelengths become[22]

$$\lambda_{m1,m2} = 2\pi/q_{m1,m2} = 2\pi\sqrt{\frac{2\alpha}{\gamma - \delta/u_{m1,m2}}}, \tag{6}$$

where $u_{m1,m2}$ satisfy

$$4\alpha u_{m1,m2}^2(2u_{m1,m2} - \kappa) = (\gamma u_{m1,m2} - \delta)^2. \tag{7}$$

The symmetry-breaking instability domain is illustrated in Fig. 2. When the aridity parameter is small, the uniform cover u_+ is stable. When the aridity parameter η is increased, the biomass is decreased, and a portion of the homogeneous cover becomes unstable. This instability occurs in the range $\eta_{m1} < \eta < \eta_{m2}$. The instability domain is bounded in the parameter space by $u_{m1,m2}$. These thresholds are linked to the aridity parameter η through the homogeneous steady state Eq. (5): $\eta_{m1,m2} = (\kappa - u_{m1,m2})u_{m1,m2}$. In Fig. 3, we plot the marginal stability curve showing the wavenumber $q_\pm^2$ corresponding to the growing Fourier modes as a function of the aridity parameter. The critical wavenumber is obtained when $q_+ = q_-$. This condition indicates that there two symmetry-breaking instability having different wavelengths, $\lambda_{m1} = 2\pi/q_{m1}$ and $\lambda_{m2} = 2\pi/q_{m2}$. The wavelength at both bifurcation points is given by Eq. (6), which determines the spatial periodicity which is defined as the distance separating the middle of two successive patches of dense vegetation. This quantity is intrinsic and it is determined only by the system's parameters and not by spatial variation of the environment or other external effects such as a dominant wind or human activities.

Two remarks are, however, necessary: First, the fact that the wavenumber q_{m1} is smaller than q_{m2} indicates that the wavelength increases when the aridity increases. This fact is in agreement with field observations. The second remark is that the change of the sign of the coefficient of the Laplace operator in the model [see Eq. (3)] constitutes the necessary condition for the destabilization of the homogeneous cover and leads to the spontaneous formation of vegetation pattern.

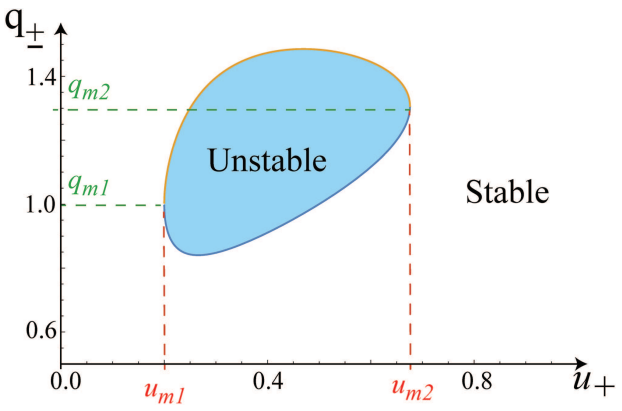

FIG. 3. The marginal stability curve in the plane $(q_\pm^2, u_+)$. The domain of instability is indicated by a shaded area. As biomass is creases two symmetry-breaking instability occurs for the parameters $\kappa = -0.1, \gamma = 2, \delta = 0.2$, and $\alpha = 0.5$. For these parameters, the thresholds are $\eta_{m1} = -0.52$, $u_{m1} = 0.68$ $\eta_{m2} = -0.05$, and $u_{m2} = 0.20$.

III. WEAKLY NONLINEAR ANALYSIS

The linear stability analysis of Sec. II shows an exponential growing solution above the threshold associated with the modulation instability. In the long time evolutions, these solutions should be non-physical. However, in this analysis, the nonlinear terms are neglected, and nonlinear effects balance this exponential growth leading to so-called saturated nonlinear state. We start our investigation of the effect of nonlinearities on the formation of periodic structures. Our goal is to derive an amplitude equation for the fastest growing Fourier mode by using the well-known multiple space-time scale expansion.[50] For this purpose, we explore the vicinity of the Turing bifurcation by defining a small parameter which measures the distance from these instabilities. Let us consider the pattern equation and the steady state equation in the vicinity of the Turing instability. We define a small parameter $\epsilon \ll 1$, which measures the distance from both symmetry-breaking bifurcation points (η_{m1}, u_{m1}) and (η_{m1}, u_{m1}) as

$$\eta = \eta_{m1,m2} + \epsilon\eta_1 + \epsilon^2\eta_2 + \dots. \tag{8}$$

We introduce the excess variable $U(x,t)$ with respect to the homogeneous steady states u_s as $u(x,t) = u_s + U(x,t)$. Then, we expand in terms of ϵ as

$$u_s = u_T + \epsilon a_1 + \epsilon^2 a_2 + \cdots, \tag{9}$$

$$U = \epsilon u_0 + \epsilon^2 u_1 + \cdots. \tag{10}$$

We seek corrections to the steady states at the symmetry-breaking thresholds that depend slow time scale $T = \epsilon^2 t$. We replace this time scale and the all the above mentioned expansion in Eq. (3). From this, we then obtain a sequence of inhomogeneous equations for the unknown functions $u_0(x,T), u_1(x,T), \dots$. We analyze each equation by applying solvability conditions. At the leading order in ϵ,

$$\mathscr{L}u_0 = 0,$$

with

$$\mathscr{L} = \kappa - 2u_T^2 + (\delta - \gamma u_T)\partial_{xx} - \alpha u_T \partial_x^{(4)}. \tag{11}$$

This equation admits solutions of the form

$$u_0 = A_0(T)\, e^{iq_{m1,m2}x} + c.c., \tag{12}$$

with $q_{m1,m2}$ as the critical wavenumber at both symmetry-breaking instability thresholds given by Eq. (6), and $A_0(T)$ as an arbitrary function of the slow time T. The term *c.c.* represents the complex conjugate.

For the homogeneous steady states, we substitute the expansions (8) and (9) in Eq. (5). At order ϵ, we obtain

$$a_1 = \frac{-\eta_1}{\sqrt{\kappa^2 - 4\eta_T}}. \tag{13}$$

At order ϵ^2, we obtain

$$\begin{aligned}\mathscr{L}u_1 \equiv & -u_0 a_1(\kappa - 4u_T) - u_0^2(\kappa - 3u_T) \\ & + (a_1 + u_0)(\gamma\partial_{xx}u_0 + \alpha\partial_{xx}^{(4)}u_0),\end{aligned} \tag{14}$$

and from Eq. (5), we get

$$a_2 = -\frac{(\eta_1^2 + \kappa^2\eta_2 - 4\eta_2\eta_T)}{(\kappa^2 - 4\eta_T)^{3/2}}. \tag{15}$$

The application of the solvability condition leads to $a_1 = 0$, and from Eq. (13), we get $\eta_1 = 0$. Then, a_2 becomes

$$a_2 = -\frac{\eta_2}{(\kappa^2 - 4\eta_T)^{1/2}}. \tag{16}$$

The solution of the inhomogeneous problem Eq. (14) is

$$u_1 = \left(A_1(T)\, e^{iq_c x} + B_1(T)\, e^{-2iq_c x} + c.c.\right) + C_1, \tag{17}$$

with C_1 is a constant and *c.c.* the complex conjugate of the terms inside the brackets. We relate the right and left side of Eq. (14) by factoring the terms proportional to the exponential terms $e^{iq_c x}$. We get

$$\begin{aligned}B_1 &= -A_0^2 \frac{\left[\delta^2 - u_T^2\left(4\alpha\kappa + \gamma^2\right) + 12\alpha u_T^3\right]}{4u_T\left[2\Delta^2 + u_T^2(2\gamma^2 - \alpha\kappa) + 2\alpha u_T^3 - 4\gamma\delta u_T\right]}, \\ C_1 &= |A_0|^2 \frac{\left[\delta^2 - u_T^2\left(4\alpha\kappa + \gamma^2\right) + 12\alpha u_T^3\right]}{4\alpha u_T^3\,(\kappa - 2u_T)}.\end{aligned} \tag{18}$$

The application of the solvability condition at higher orders of the inhomogeneous problem, i.e., order ϵ^3, leads us to

$$\begin{aligned}\mathscr{L}u_2 = & -u_0 a_2(\kappa - 4u_T + \gamma q_c^2 - \alpha q_c^4) \\ & - u_0 u_1(2\kappa - 6u_T + \gamma q_c^2 - \alpha q_c^4) + u_0^3 \\ & + \partial_T u_0 + \gamma u_0 \partial_{xx} u_1 + \alpha u_0 \partial_x^{(4)} u_1.\end{aligned} \tag{19}$$

This yields in the following amplitude equation:

$$\begin{aligned}\partial_T A_0 = & -\frac{\eta_2}{(\kappa^2 - 4\eta_T)^{1/2}}\left(\frac{1}{4\alpha}(\gamma^2 - \delta^2/u_T^2) + \kappa - 4u_T\right)A_0 \\ & + hA_0|A_0|^2,\end{aligned} \tag{20}$$

the coefficient of the cubic term is

$$h = \Big[4\gamma^3\delta^3 + 56\alpha^3 u_T^6 + 2\alpha^2 u_T^4\left(\alpha\kappa^2 - 2\gamma^2\kappa - 50\gamma\delta\right) - 8\alpha^2 u_T^5\left(4\alpha\kappa + \gamma^2\right) + \gamma^2\delta^2 u_T\left(19\alpha\kappa - 2\gamma^2\right) - 2\alpha\gamma\delta u_T^2\left(11\alpha\kappa^2 + 5\gamma^2\kappa + 31\gamma\delta\right) + 2\alpha\gamma\delta u_T^3\left(55\alpha\kappa + 16\gamma^2\right)\Big]/\Gamma, \tag{21}$$

with $\Gamma = 2\alpha^2 u_T^3(\kappa - 2u_T)\left[-8\gamma\delta + u_T\left(7\alpha\kappa + 4\gamma^2\right) - 14\alpha u_T^2\right]$.

Let us rewrite the amplitude equation in terms of physical variables by using the time scale relations $T = \epsilon^2 t$, $A = \epsilon A_0$, and $\eta = \eta_T + \eta_2\epsilon^2$. We obtain

$$\partial_t A = -(\eta - \eta_T)gA + hA|A|^2, \tag{22}$$

with

$$g = (\kappa^2 - 4\eta_T)^{1/2}\left(\frac{1}{4\alpha}(\gamma^2 - \delta^2/u_T^2) + \kappa - 4u_T\right). \tag{23}$$

Using the polar decomposition of $A = A_s\exp(i\phi)$, yields the two steady solutions: the trivial solution $A_s = 0$ that corresponds to the homogeneous cover, and the nontrivial solution $A_{s\pm} = \pm\sqrt{(\eta - \eta_T)g/h}$. Close to the first bifurcation, $\eta > \eta_m = \eta_{m1}$, these solutions exist only if g and h have the same sign. However, close to the second bifurcation point, $\eta > \eta_m = \eta_{m2}$, the solution $A_{s\pm}$ exists when g and h have opposite sign. In both cases, the symmetry-breaking bifurcation appears supercritically. The branch of periodic vegetation patterns solution of the amplitude equation $A_{s\pm}$ that emerges from both cases is stable when close to the bifurcation point. This solution exists for $\eta_{m1} < \eta < \eta_{m2}$.

We fix $\kappa = -0.1$, $\gamma = 2$, $\delta = 0.2$, and $\alpha = 0.5$. Let the aridity η be the control parameter. For these parameters, there are two symmetry-breaking bifurcations: $(\eta_{m1} = -0.52, u_{m1} = 0.68)$ and $(\eta_{m2} = -0.05, u_{m2} = 0.20)$. The wavelength at both bifurcations is given by $\Lambda_{m1} = 2\pi/q_{m1} = 4.81$ and $\Lambda_{m2} = 2\pi/q_{m2} = 6.28$. The corresponding amplitude equation becomes

$$\text{For } \eta > \eta_{m1}: \quad \partial_t A = 0.58(\eta - \eta_{m1})A - 2.7A|A|^2, \tag{24}$$

$$\text{For } \eta < \eta_{m2}: \quad \partial_t A = -1.2(\eta - \eta_{m2})A - 27.17A|A|^2. \tag{25}$$

In addition to the homogeneous cover $A_s = 0$, the stationary periodic solutions of the amplitude equation are $A_{s\pm} = \pm\sqrt{0.21(\eta - \eta_{m1})}$ and $A_{s\pm} = \pm\sqrt{-0.04(\eta - \eta_{m1})}$. These results indicate that both bifurcation appear supercritically. To check these results, we perform numerical simulations of the interaction-redistribution model Eq. (1) using periodic boundary conditions. The results are shown in the bifurcation diagram of Fig. 4. The homogeneous cover undergoes two symmetry-breaking bifurcation located at $\eta_{m1} = -0.52$ and $\eta_{m2} = -0.05$. Both bifurcations arise supercritically and are connected by a branch of periodic solutions as shown in Fig. 4. The extrema of the emerging vegetation patterns are represented by dotted curves. The transition from supercritical to subcritical occurs when the function h, the coefficient of the cubic term in the amplitude equation, vanishes (see Fig. 5). The white lines represent zones in which h diverges. This

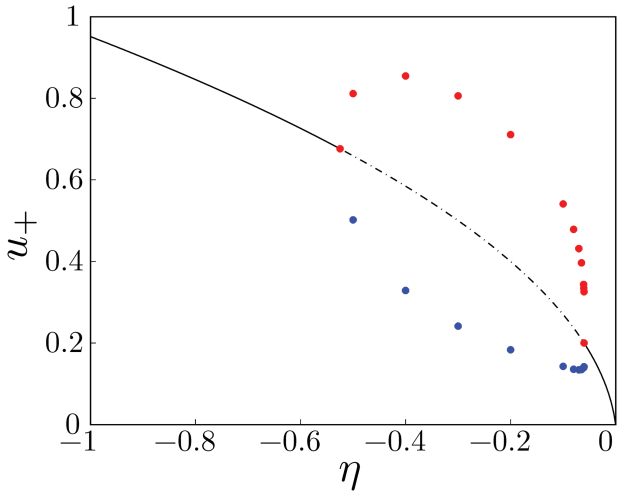

FIG. 4. Bifurcation diagram of steady state solution u_+ obtained for parameters $\kappa = -0.1$, $\gamma = 2$, $\delta = 0.2$, and $\alpha = 0.5$. The full and broken lines correspond to stable and unstable states, respectively. The maxima and the minima of u_+ during the unstable phase are indicated by dots. Numerical simulation of Eq. (3) are obtained by using periodic boundary conditions. The initial condition consists of a small amplitude noise added to the unstable homogeneous cover.

occurs when $\Gamma = 0$, which takes place at values $u_T^{(1)} = 0$, $u_T^{(2)} = \kappa/2$, and

$$u_T^{(3)} = \frac{4\gamma^2 + 7\alpha\kappa - \sqrt{(4\gamma^2 + 7\alpha\kappa)^2 - 488\alpha\gamma\delta}}{28\alpha}, \qquad u_T^{(4)} = \frac{4\gamma^2 + 7\alpha\kappa + \sqrt{(4\gamma^2 + 7\alpha\kappa)^2 - 488\alpha\gamma\delta}}{28\alpha}. \tag{26}$$

Notice $u_T^{(3)}$ and $u_T^{(4)}$ can become complex numbers. In such cases we discard them.

The above weakly nonlinear analysis have been performed in the case of one-dimensional system. In two dimensions, numerical simulations of Eq. (3) support a well-known scenario: as the aridity increases, the symmetry of vegetation patterns transforms from π-hexagons into stripes and, finally, into 0-hexagons. This generic scenario and the associated pattern selection have been predicted in Refs. 5, 19, and 22. The maximum and minimum biomass densities for these three types of the two-dimensional vegetation patterns are plotted in Fig. 6 as a function of the aridity parameter for fixed values of the cooperativity and the canopy-to-rhizosphere radius ratio. This diagram has been obtained using a truncated Fourier series expansion.[19]

IV. LOCALIZED VEGETATION PATCHES FORMATION

In this section, we focus on a regime where symmetry-breaking instability appears supercritically. We consider a bistable regime, where $\kappa = 1$ (i.e., it is positive), we fix the parameters $\delta = 0.02$,

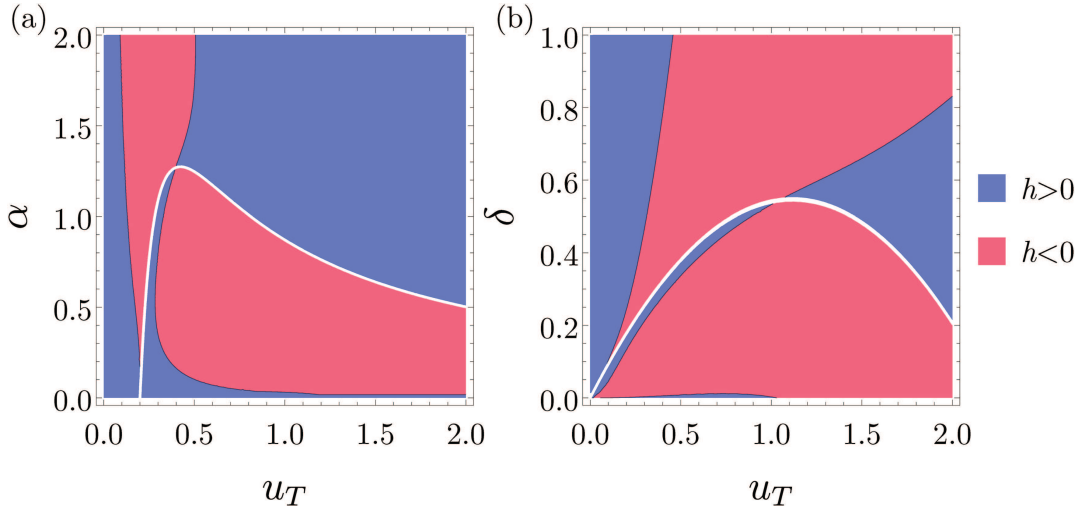

FIG. 5. Regions in which the coefficient h [see Eq. (22)] has positive or negative sign. We set parameters $\kappa = -0.1$, $\gamma = 2$, and $\delta = 0.2$ for panel (a) and $\alpha = 0.5$ for panel (b). The white lines represent zones in which h diverges. For the parameters used here they correspond to terms $u_T^{(3)}$ and $u_T^{(4)}$ in Eq. (26).

$\gamma = 0.5$, $\alpha = 0.1$, and let the aridity parameter, η, be the control parameter. For this set of parameters, there exists a single symmetry-breaking instability point located on the homogeneous cover u_+. At this bifurcation point, the aridity, as well as the corresponding biomass, can be calculated from Eqs. (7) and (5) from

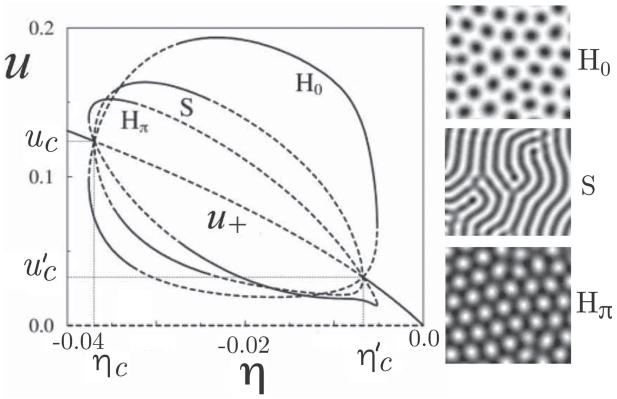

FIG. 6. Bifurcation diagram of model Eq. (3) obtained for the monostable regime ($\eta = -0.175 < 0$) as a function of the aridity parameter η. Others parameters are $\delta = 0.005$, $\gamma = 0.5$, and $\alpha = 0.25$. The sequence hexagons H_π, stripes S, and the hexagons H_0 are obtained for $\eta = -0.035$, $\eta = -0.03$, and $\eta = -0.02$, respectively. These two-dimensional structures have been obtained by direct numerical simulation of Eq. (3) using the finite differences scheme with Runge–Kutta order-4 algorithm with periodic boundary conditions. Black color corresponds to the highest biomass density. Reproduced with permission from Lejeune *et al.*, Int. J. Quantum Chem. **98**, 261 (2004). Copyright 2004 John Wiley and Sons.

which we obtain $\eta_m = -0.61$ and $u_m = 0.78$. These values are estimated accurately to two decimal places. As the aridity parameter is increased, we recover the well-known sequence of vegetation pattern π-hexagons stripes-0-hexagons mentioned above. In what follows, we focus on the regime where the bare state coexists with a periodic vegetation pattern of the 0-hexagons symmetry as shown in Fig. 7(a). Both states are stable within a finite range of the aridity parameter $0 < \eta < 0.35$. In this regime, when we perturb a system in a small area located in the center of the integration domain with large biomass density, the system evolves to the formation of a single patch of vegetation as shown in Fig. 7(b).

The corresponding cross section along the x-direction is shown in Fig. 7(c). The localized patch possesses a circular shape surrounded by a bare state. The stationary localized patch has been interpreted as a nonlinear front that undergoes a pinning effect between the periodic vegetation pattern and the bare state.[20] This mechanism leading to the formation of localized structures and localized patterns is well known in other class of spatially extended systems.[51–59]

The size of a single patch neither grows despite available free space nor decreases despite harsh environmental conditions.[20] The maximum biomass density obtained at the center of the localized patch is approximately equal to the one corresponding to the hexagonal spatially periodic pattern. The width of this localized state is the half of wavelength at the symmetry-breaking instability provided by Eq. (6). To compare with analytical results, we first calculate the width given by the linear stability analysis [see Eq. (6) from Sec. II], so the width of localized patch is $\lambda_m/2 = \pi\sqrt{2\alpha/(\gamma/u_m - \delta)}$ ≈ 2.04), while the width of stable patch obtained numerically is ≈ 2.23. We see a good agreement with the half-wavelength and the width of the isolated patch. A single patch is not stable in all the range where the system undergoes a coexistence between the bare

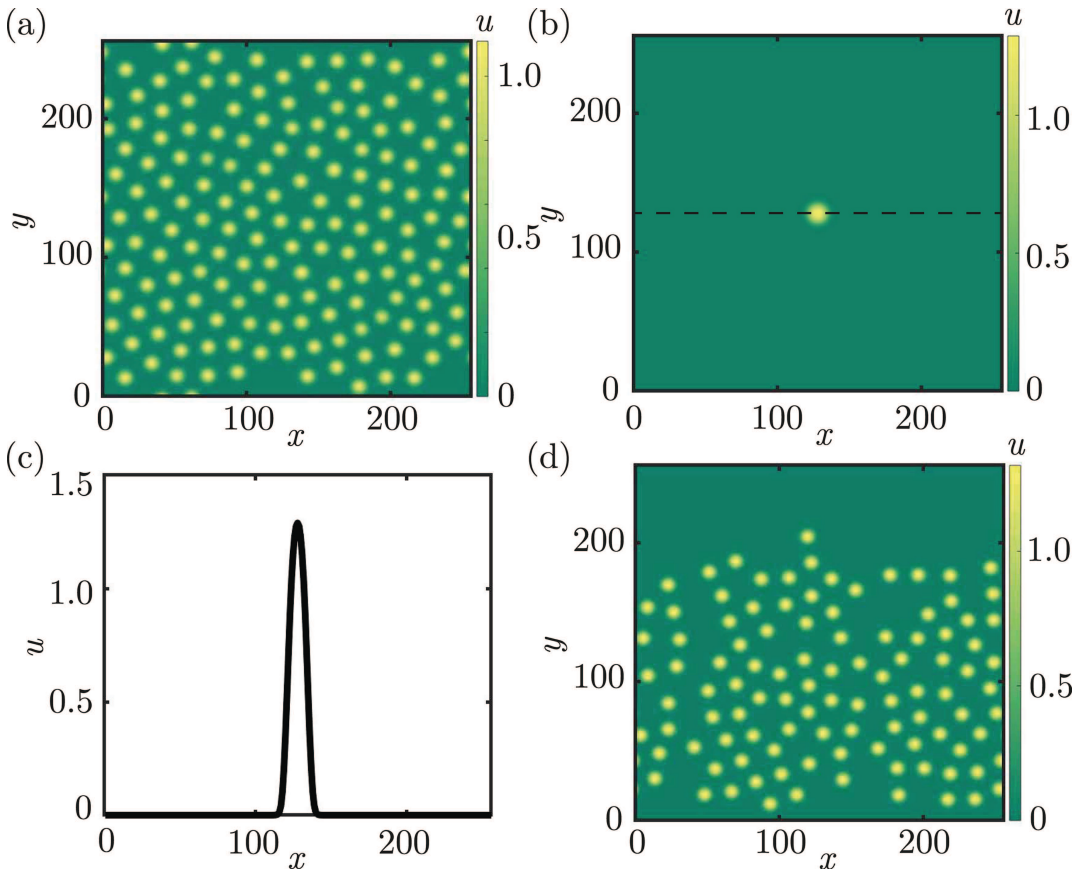

FIG. 7. Vegetation patterns obtained from numerical simulation of the interaction-redistribution model given by Eq. (3). Parameters used $\kappa = 1, \delta = 0.02, \gamma = 0.5, \alpha = 0.1$, and $\eta = 0.3$. (a) Periodic vegetation pattern in which the bare state coexists with 0-hexagons. The initial condition consists of perturbing the stable bare state at form grid point located at the center of the integration domain. The amplitude of the perturbation is $b = 2$. (b) Single localized patch. (c) Cross section taken from the dashed line along the x-direction in (b) passing through the center of the patch. (d) Multi-spot structure of randomly located spots. In panels (a), (b), and (d), the maxima are plain yellow and mesh number integration is 256×256.

state and the hexagonal periodic structures, i.e., $0 < \eta < 0.35$. It is stable in the range called the pinning zone of the aridity parameter $0.26 < \eta < 0.35$. Therefore, the coexistence between these two qualitatively states is a necessary but not a sufficient condition for the stability of a single patch solution.

As the wavelength is intrinsic, the width or the size of localized patches is also intrinsic to the dynamics of the system. Another interesting property of localized patches is that the tail decays as a function of distance without oscillations. In fact, field observations show that each patch is surrounded by bare soil [see Fig. 1(a)]. In this case, it has been shown recently that the interaction between vegetation patches is always repulsive.[60,61] Therefore, bounded states and clusters of vegetation patches are not stable. An example of a localized vegetation pattern involving multi-spot structure is shown in Fig. 7(d). The repulsive interaction evolves on a longer time scale comparing to the time scale of the formation of periodic vegetation patterns. Over time, this localized pattern will reach either a periodic structure or superlattice type of structures.[60] Note that contrarily to patches, localized gaps have an oscillatory exponentially decaying tails. When two gaps are well-separated, the interaction between them alternates between attractive and repulsive. In this case, bounded states and clusters of gaps can be stable.[22] By using the continuation method based on the pseudo-arc length technique, it has been shown that these gaps undergo a homoclinic snaking type of bifurcation.[62]

When decreasing the aridity parameter with $\eta < 0.26$, the patches lose their circular shape and exhibit elliptical deformation leading to elongation of localized patches of vegetation. The instability leading to the deformation of the circular shape of localized patches is regularly called self-replication.[34–36] During this process, each patch splits into two new patches, as shown in Ref. 34. However, in the range of parameters considered in this contribution, the patch exhibits an elliptical deformation but they do not split. Instead, they rather elongate to form a rodlike localized state. The

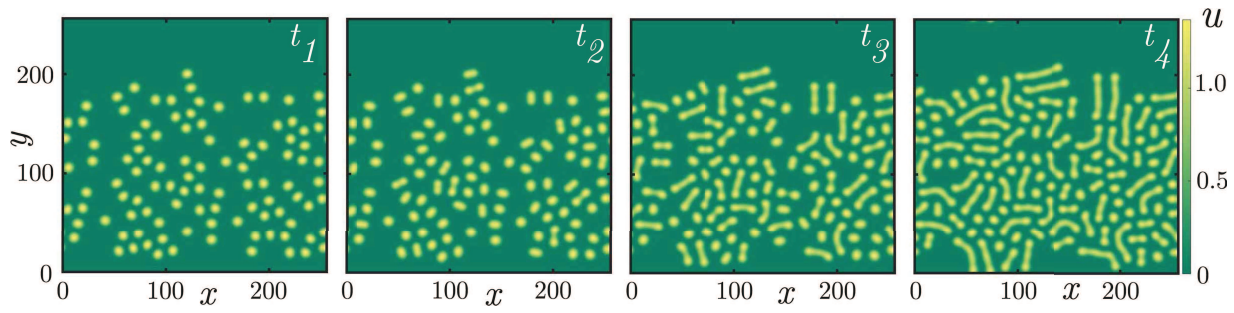

FIG. 8. Time evolution of vegetation pattern $t_1 < t_2 < t_3 < t_4$. Parameters are $\kappa = 1$, $\delta = 0.02$, $\gamma = 0.5$, $\alpha = 0.1$, and $\eta = 0.25$. Maxima are plain yellow and mesh number integration is 256×256.

time evolution of this phenomenon is shown in Fig. 8. This behavior is a well-documented issue in other fields of nonlinear science.[63]

V. DISCUSSION AND CONCLUSION

We have considered the interaction-redistribution model Eq. (1) describing the spatiotemporal evolution of the biomass that takes into account the facilitative and competitive interactions between individual plants and seed dispersion. We have summarized the reduction of this integrodifferential model to a simple partial differential equation based upon the weak gradient limit, Eq. (3). In this limit, around the critical point (i.e., in the neighborhood of the tipping point), the system exhibits bistability, and long-wavelength pattern forming regime. We have assumed that the Kernels associated with facilitative-competitive and seed dispersion are Gaussians and considered environmental conditions as strictly homogeneous and isotropic. Under these conditions, we have performed a weakly nonlinear analysis of the reduced model in the neighborhood of both symmetry-breaking instabilities. This allowed us to derive conditions for transitions from a supercritical to subcritical symmetry-breaking instability.

The weakly nonlinear analysis allowed us to determine the threshold associated with the formation of localized patches of vegetation. This threshold is given by the condition $h = 0$, with h bing the coefficient of the cubic term in the amplitude equation given by Eq. (22). Above this threshold, the symmetry-breaking bifurcation becomes subcritical and leads to the coexistence of bare state and spatially periodic vegetation patterns both of which are stable for a finite range of the aridity parameter. This coexistence is a prerequisite for the formation of localized vegetation patches. Such localized vegetation patterns in arid ecosystems are interpreted as an outcome of a subcritical symmetry-breaking mechanism. We have characterized localized vegetation structures by estimating the maximum peak biomass and its width. Out of the pinning region (where a single patch is stable), we have identified an instability which leads to the formation of rodlike structures for intermediate values of the aridity parameters. We have shown that these rodlike structures coexist with circular patches of vegetation.

A major challenge in plant ecology lies in the model parameterization and in assessing the role of parameters in vegetation dynamics. Field measurements have been carried out on the *Stipa tenacissima L.* plant, a drought-resistant plant belonging to the Gramineae family. This species originates from the arid regions of western of the Mediterranean basin; its range extends to Spain, Portugal, Balearic Islands, and North Africa in the highlands of Morocco, Algeria, and Egypt passing through Tunisia and Libya. Characteristics of the *Stipa tenacissima L.* plant such as height, aerial diameter, and biomass can be found in Ref. 64. It has been reported that lateral roots track water far beyond the limits of the rhizosphere radius.[65–68]

The alfa plants grow in both calcareous and siliceous soils or even in sands, and its biomass can reach 3, 157, 143 tufts per hectare. Field measurements have been conducted in the center-south of Morocco, in the commune Enjil attached to Fez-Meknès Region, at 2029 m of altitude. This region is characterized by an average annual temperature of around 20.5 °C with a daily minimum of 3 °C and daily maximum of 38 °C on average. The annual precipitations range between 300 and 400 mm/year. In these arid zones, vegetation is not uniformly distributed in space but appears as small clusters of plants interspersed with bare soil areas. An example of such behavior is plotted in Fig. 1(a).

We have measured both the facilitation- and competition-interaction lengths of the alfa plant. The biomass density was quantified by measuring the net biomass (in kilograms) both above and below the ground surface, normalizing them with their respective surface areas governed by the facilitative and competitive lengths. When alfa plants are to water drought, they extend their roots beyond the radius of the above-ground. This spreading of their roots over a larger territory is essential for the survival against evapotranspiration. The lateral expansion of roots increases the water and nutrient uptake of the alfa plant. From our measurements, we obtained an average aerial radius of $L_f = 57.3$ cm and an average root radius of $L_c = 180.1$ cm. The average measurements of the above- and below-ground biomass density resulted in 1494.3 g/m^2 and 197.7 g/m^2, respectively.

To make a connection between the measured lengths associated with the facilitative L_f and the competitive L_c interactions and their link to the parameters that appear in the model [see Eq. (3)], we rewrite the relations in Eq. (4) by expressing the dependence of the parameters δ, γ, and α on the two lengths, i.e., $\delta = pL_f^2/(2L_d^2)$,

$\gamma = \chi(L_f^2/L_c^2 - 1)/2$, and $\alpha = L_c^2/(16L_f^2)$. We see from these relations that only the parameter $\alpha = L_c^2/(16L_f^2)$ can be estimated from our field observations. Using the values reported above, this results in $\alpha = 180.1^2/(16 * 57.3^2) \approx 0.6$. To estimate the values of the δ, γ, it would be necessary to measure the length L_d and the diffusion coefficient p of the seed dispersion. Another parameter that would need to be measured is the strength of the interactions χ. More data on this ecosystem, coupled with a new campaign of field measurements is, therefore, necessary to perform a full parameterization and parameter assessment for these types of arid ecosystems. This would allow us to perform a quantitative comparison of the threshold as well as the wavelength of the vegetation pattern observed arid landscape. It is, however, beyond the scope of this contribution to compare quantitatively the analytical results obtained using the proposed model with field observations.

ACKNOWLEDGMENTS

We would like to thank R. Lefever for helpful interactions. We are grateful to S.S. Gopalakrishnan for his continuous help. M.G.C. thanks for financial support of FONDECYT projects 1180903 and Millennium Institute for Research in Optics (MIRO). E.B. thanks financial support of CONICYT through Becas Magister Nacional 2015, Contract No. 22151824. M.T. received support from the Fonds National de la Recherche Scientifique (Belgium). The authors gratefully acknowledge financial support of Wallonie-Bruxelles International (WBI).

DATA AVAILABILITY

The data that support the findings of this study are available from the corresponding author upon reasonable request.

REFERENCES

[1] S. A. Levin, Ecology **73**, 1943 (1992).
[2] P. Greig-Smith, J. Ecol. **67**, 755 (1979).
[3] K. A. Kershaw, Ecology **44**, 377 (1963).
[4] R. Lefever and O. Lejeune, Bull. Math. Biol. **59**, 263 (1997).
[5] O. Lejeune and M. Tlidi, J. Veg. Sci. **10**, 201 (1999).
[6] R. Lefever and J. Turner, C. R. Mec. **340**, 818 (2012).
[7] R. M. Callaway, Bot. Rev. **61**, 306 (1995).
[8] R. M. Callaway and L. R. Walker, Ecology **78**, 1958 (1997).
[9] N. Barbier, P. Couteron, R. Lefever, V. Deblauwe, and O. Lejeune, Ecology **89**, 1521 (2008).
[10] R. Lefever, N. Barbier, P. Couteron, and O. Lejeune, J. Theor. Biol. **261**, 194 (2009).
[11] P. Couteron, F. Anthelme, M. Clerc, D. Escaff, C. Fernandez-Oto, and M. Tlidi, Philos. Trans. R. Soc. A **372**, 20140102 (2014).
[12] C. A. Klausmeier, Science **284**, 1826 (1999).
[13] R. HilleRisLambers, M. Rietkerk, F. van den Bosch, H. H. Prins, and H. de Kroon, Ecology **82**, 50 (2001).
[14] T. Okayasu and Y. Aizawa, Prog. Theor. Phys. **106**, 705 (2001).
[15] J. von Hardenberg, E. Meron, M. Shachak, and Y. Zarmi, Phys. Rev. Lett. **87**, 198101 (2001).
[16] E. Gilad, J. von Hardenberg, A. Provenzale, M. Shachak, and E. Meron, Phys. Rev. Lett. **93**, 098105 (2004).
[17] E. Winkler and S. Klotz, J. Veg. Sci. **8**, 189 (1997).
[18] W. A. Macfadyen, Geogr. J. **116**, 199 (1950).
[19] O. Lejeune, M. Tlidi, and R. Lefever, Int. J. Quantum Chem. **98**, 261 (2004).
[20] O. Lejeune, M. Tlidi, and P. Couteron, Phys. Rev. E **66**, 010901 (2002).
[21] M. Rietkerk, S. C. Dekker, P. C. De Ruiter, and J. van de Koppel, Science **305**, 1926 (2004).
[22] M. Tlidi, R. Lefever, and A. Vladimirov, Lect. Notes Phys. **751**, 381 (2008).
[23] M. Van Rooyen, G. Theron, N. Van Rooyen, W. Jankowitz, and W. Matthews, J. Arid Environ. **57**, 467 (2004).
[24] W. R. Tschinkel, PLoS One **7**, e38056 (2012).
[25] M. D. Cramer and N. N. Barger, PLoS One **8**, e70876 (2013).
[26] N. Juergens, Science **339**, 1618 (2013).
[27] C. Fernandez-Oto, M. Tlidi, D. Escaff, and M. Clerc, Philos. Trans. R. Soc. A **372**, 20140009 (2014).
[28] C. Fernandez-Oto, M. Clerc, D. Escaff, and M. Tlidi, Phys. Rev. Lett. **110**, 174101 (2013).
[29] D. Escaff, C. Fernandez-Oto, M. Clerc, and M. Tlidi, Phys. Rev. E **91**, 022924 (2015).
[30] S. Getzin, K. Wiegand, T. Wiegand, H. Yizhaq, J. von Hardenberg, and E. Meron, Ecography **38**, 1 (2015).
[31] M. D. Picker, V. Ross-Gillespie, K. Vlieghe, and E. Moll, Ecol. Entomol. **37**, 33 (2012).
[32] J. A. Bonachela, R. M. Pringle, E. Sheffer, T. C. Coverdale, J. A. Guyton, K. K. Caylor, S. A. Levin, and C. E. Tarnita, Science **347**, 651 (2015).
[33] C. E. Tarnita, J. A. Bonachela, E. Sheffer, J. A. Guyton, T. C. Coverdale, R. A. Long, and R. M. Pringle, Nature **541**, 398 (2017).
[34] I. Bordeu, M. G. Clerc, P. Couteron, R. Lefever, and M. Tlidi, Sci. Rep. **6**, 33703 (2016).
[35] I. Bordeu, M. Clerc, R. Lefever, and M. Tlidi, Commun. Nonlinear Sci. Numer. Simul. **29**, 482 (2015).
[36] M. Tlidi, I. Bordeu, M. G. Clerc, and D. Escaff, Ecol. Indic. **94**, 534 (2018).
[37] M. Tlidi, M. Clerc, D. Escaff, P. Couteron, M. Messaoudi, M. Khaffou, and A. Makhoute, Philos. Trans. R. Soc. A **376**, 20180026 (2018).
[38] F. T. Arecchi, S. Boccaletti, and P. Ramazza, Phys. Rep. **318**, 1 (1999).
[39] K. Staliunas and V. J. Sanchez-Morcillo, *Transverse Patterns in Nonlinear Optical Resonators* (Springer Science & Business Media, 2003), Vol. 183.
[40] *Dryland ecohydrology*, edited by P. D'Odorico, A. Porporato, and C. W. Runyan (Springer, Dordrecht, 2006).
[41] M. Tlidi, M. Taki, and T. Kolokolnikov, "Introduction: Dissipative localized structures in extended systems," Chaos **17**, 037101 (2007).
[42] *Dissipative Solitons: From Optics to Biology and Medicine*, edited by N. Akhmediev and A. Ankiewicz (Springer Science & Business Media, 2008).
[43] O. Descalzi, M. Clerc, S. Residori, and G. Assanto, *Localised States in Physics: Solitons and Patterns* (Springer Science & Business Media, 2011).
[44] M. Tlidi, K. Staliunas, K. Panajotov, A. G. Vladimirov, and M. G. Clerc, Philos. Trans. R. Soc. A **372**, 20140101 (2014).
[45] E. Meron, *Nonlinear Physics of Ecosystems* (CRC Press and Taylor & Francis Group, 2015).
[46] M. Tlidi and M. G. Clerc, *Nonlinear Dynamics: Materials, Theory and Experiments*, Springer Proceedings in Physics Vol. 173 (Springer, New York, 2016).
[47] Y. K. Chembo, D. Gomila, M. Tlidi, and C. R. Menyuk, Eur. Phys. J. D. **71**, 299 (2017).
[48] M. Tlidi and K. Panajotov, Rom. Rep. Phys. **70**, 406 (2018), available at http://www.rrp.infim.ro/IP/2018/AN406.pdf.
[49] M. Tlidi, M. Clerc, and K. Panajotov, Philos. Trans. R. Soc. A **376**, 20180114 (2018).
[50] J. K. Kevorkian and J. D. Cole, *Multiple Scale and Singular Perturbation Methods* (Springer Science & Business Media, 2012).
[51] S. Koga and Y. Kuramoto, Prog. Theor. Phys. **63**, 106 (1980).
[52] Y. Pomeau, Physica D **23**, 3 (1986).
[53] M. Tlidi, P. Mandel, and R. Lefever, Phys. Rev. Lett. **73**, 640 (1994).
[54] O. Jensen, V. O. Pannbacker, E. Mosekilde, G. Dewel, and P. Borckmans, Phys. Rev. E **50**, 736 (1994).
[55] A. R. Champneys, Physica **112D**, 158 (1998).
[56] P. Coullet, C. Riera, and C. Tresser, Phys. Rev. Lett. **84**, 3069 (2000).
[57] M. G. Clerc and C. Falcon, Physica **356A**, 48 (2005).
[58] M. G. Clerc, C. Falcon, and E. Tirapegui, Phys. Rev. Lett. **94**, 148302 (2005).

[59]M. G. Clerc, C. Falcon, and E. Tirapegui, Phys. Rev. E **74**, 011303 (2006).
[60]E. Berríos-Caro, M. G. Clerc, D. Escaff, C. Sandivari, and M. Tlidi, Sci. Rep. **10**, 1 (2020).
[61]M. Tlidi, E. Berríos-Caro, D. Pinto-Ramo, A. G. Vladimirov, and M. Clerc, "Interaction between vegetation patches and gaps: A self-organized response to water scarcity," Physica D (published online 2020).
[62]J. Cisternas, D. Escaff, M. G. Clerc, R. Lefever, and M. Tlidi, Chaos Solitons Fractals **133**, 109617 (2020).
[63]I. Bordeu and M. G. Clerc, Phys. Rev. E **92**, 042915 (2015).
[64]K. Aloui, M. Ksontini, and M. Néjib Rejeb, Ann. l'Inrgref **18**, 213 (2013).
[65]A. J. Belsky, Ecology **75**, 922 (1994).
[66]H. J. Schenk and R. B. Jackson, J. Ecol. **90**, 480 (2002).
[67]N. Barbier, P. Couteron, J. Lejoly, V. Deblauwe, and O. Lejeune, J. Ecol. **94**, 537 (2006).
[68]S. N. Martens, D. D. Breshears, C. W. Meyer, and F. J. J. Barnes, J. Veg. Sci. **8**, 655 (1997).